


Deep subwavelength imaging via tunable terahertz plasmons

Cite as: Appl. Phys. Lett. **113**, 051106 (2018); <https://doi.org/10.1063/1.5035312>

Submitted: 14 April 2018 . Accepted: 23 July 2018 . Published Online: 03 August 2018

Hasan Tahir Abbas , Xiaodong Zeng, Robert D. Nevels, and M. Suhail Zubairy



View Online



Export Citation



CrossMark

ARTICLES YOU MAY BE INTERESTED IN

[Half-cycle terahertz surface waves with MV/cm field strengths generated on metal wires](#)

Applied Physics Letters **113**, 051101 (2018); <https://doi.org/10.1063/1.5031873>

[Terahertz metamaterial perfect absorber with continuously tunable air spacer layer](#)

Applied Physics Letters **113**, 061113 (2018); <https://doi.org/10.1063/1.5041282>

[Polarization-controlled terahertz super-focusing](#)

Applied Physics Letters **113**, 071102 (2018); <https://doi.org/10.1063/1.5039539>



**THE WORLD'S RESOURCE FOR
VARIABLE TEMPERATURE
SOLID STATE CHARACTERIZATION**



WWW.MMR-TECH.COM

OPTICAL STUDIES SYSTEMS

SEEBECK STUDIES SYSTEMS

MICROPROBE STATIONS

HALL EFFECT STUDY SYSTEMS AND MAGNETS

Deep subwavelength imaging via tunable terahertz plasmons

Hasan Tahir Abbas,^{1,2} Xiaodong Zeng,^{3,a)} Robert D. Nevels,¹ and M. Suhail Zubairy^{3,b)}

¹Department of Electrical and Computer Engineering, Texas A & M University, College Station, Texas 77843 USA

²Department of Electrical and Computer Engineering, Texas A & M University at Qatar, Doha, Qatar

³Institute for Quantum Science and Engineering (IQSE) and Department of Physics and Astronomy, Texas A & M University, College Station, Texas 77843-4242, USA

(Received 14 April 2018; accepted 23 July 2018; published online 3 August 2018)

A deep subwavelength structured illumination microscopy scheme via tunable plasmons is proposed. The sample is placed on a semiconductor heterostructure where terahertz plasmons generated by a current-driven instability illuminate it. Full coverage of the spatial frequency regime is obtained by tuning the plasmons through adjusting gate voltage. Hence, it is possible to reconstruct an image with a resolution down to 75 nm and up to two orders of magnitude beyond the diffraction limit. Due to the linear nature of the technique, only a weak illumination signal is required, which minimizes the likelihood of sample damage and has potential applications in bioimaging.

Published by AIP Publishing. <https://doi.org/10.1063/1.5035312>

In conventional wide-field fluorescence microscopy, the resolution of the system is half the wavelength of light due to the Abbe diffraction limit. With an ever growing need to image minuscule objects especially in life sciences, several superresolution microscopies have been realized. Structured illumination microscopy (SIM)^{1–5} is a wide-field technique in which a fine illumination pattern such as a sinusoidal standing wave is used to generate *Moiré fringes* in the observed image.^{2,3} The high spatial frequency content is mathematically reconstructed from a series of images acquired by shifting the pattern. Theoretically, unlimited resolution can be achieved using a non-linear version of SIM.⁴ However, the requirement of high-level illumination intensity subjects the sample to significant damage, induced by thermal and bleaching effects. It has been found that resolution beyond the classical diffraction limit by a factor greater than 2 can be realized when an object is illuminated by surface and localized plasmons,^{6–11} which have much smaller wavelengths.

Current-driven plasmon instabilities have mainly been studied in the context of ionized gases for a long time.¹² An analogous activity leads to the generation of plasmons in solid-state devices that have many interesting applications in the far-infrared frequency region.^{13–23} More importantly, and interestingly, the spatial frequency response of the device can be tuned by varying the gate voltage.^{24,25} In this paper, a deep subwavelength imaging technique is proposed where terahertz plasmons, generated by a current in a transistor channel that can be tuned by controlling gate voltage, form the illumination pattern required for SIM. This configuration effectively creates a much larger observable spatial frequency region as compared to that of a terahertz wave. Due to the linear nature of the scheme, a resolution of up to two orders of magnitude beyond the diffraction limit can be obtained with a weak field intensity, which produces little damage to the sample and may play an important role in

bioimaging. In comparison with the metal based SIM where the plasmonic wavelength is fixed by a determined structure,⁶ the period of the plasmonic pattern can be controlled by varying the gate voltage. Moreover, in contrast to a previous scheme based on graphene,¹¹ our method uses surface current to excite the plasmons, which avoids any wavevector matching mechanism such as a grating. Thus, our scheme can be realized in experiment more easily.

A schematic diagram of the proposed system, which is similar to a transistor, is shown in Fig. 1 where a two dimension electron gas (2DEG) acting as a transistor channel is formed at the interface of two semiconductor materials with slightly different band-gap energies. Plasmons are generated in the channel when the source and drain terminals are driven by a current source. Due to reflections from the conducting boundaries, the channel region creates a cavity where the plasmons form a standing wave. The structure is backed by a gate terminal that spans the length L of the channel and is spaced a distance d below the 2DEG. The gate capacitively couples with the 2DEG, and so, the velocity as well as the concentration of electrons in the channel can be controlled by varying the gate voltage. A barrier layer of thickness h separates the sample from the 2DEG.

The compressed nature of the plasmons can be described by their dispersion relation. Here, we consider the sample

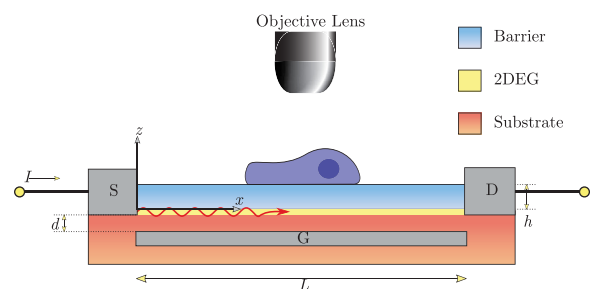


FIG. 1. Illustration of the imaging scheme where the sample is excited by the standing plasmonic wave pattern generated in the 2DEG by a current-driven instability. Transistor arrangement with S, D, and G denoting the source, drain, and gate.

^{a)}Electronic mail: zengxdgood@163.com

^{b)}Electronic mail: zubairy@physics.tamu.edu

stage which is terminated by a gate at the bottom and free-space at the top.^{26,27} The 2DEG is modeled as a shunt admittance related to Drude-type surface conductivity,²⁸ $\sigma_s = N_s e^2 \tau / [m^* (1 - j\omega_p \tau)]$, where N_s is the surface electron density in the channel, e is the electron charge, m^* is the effective electron mass in the heterostructure, τ is the scattering time of electrons, and ω_p is the angular frequency. Through the gate voltage V_g , the electron density N_s of the channel can be varied as $N_s = N_0 (1 - V_g/V_T)$, where $N_0 = \epsilon_2 \epsilon_0 V_T / ed$ is the zero-bias density, V_T is the gate threshold voltage of the transistor, and ϵ_2 is the relative permittivity of the semiconductor substrate. The plasmonic dispersion relation can be written as $1 - r_u r_d e^{-2k_p h} = 0$. Here, r_u accounts for the reflection from the barrier to the vacuum, while r_d refers to the reflection from the barrier to the substrate with 2DEG between them. Figure 2 shows that the plasmonic wave number can be controlled by varying the gate voltage. The result is similar to the dispersion curve of the gated 2DEG plasmons where the gate terminal is located above the barrier.^{29,30} Here, the permittivity of both semiconductor layers is approximated to the static value, i.e., $\epsilon_1 \approx \epsilon_2 = 9.5$; the plasmon frequency is 10 THz; the mole-fraction of aluminum in AlGaIn alloy is 0.1; and the scattering time τ is 1.14 ps corresponding to a temperature of 77 K.³¹ As the temperature is increased, τ gets smaller which leads to reduced mobility and induces larger loss in the channel. Compared to the vacuum wavenumber of 2.09×10^5 rad/m, the figure demonstrates that the plasmonic wave vector can be hundreds of times larger than that in vacuum. A sample observed through such a high subwavelength illumination makes superresolution possible.

As discussed before, the 2DEG channel essentially behaves as a cavity due to the resonance effects introduced by the two conducting boundaries, i.e., drain and source terminals. Therefore, the plasmonic wavenumber k_p cannot be varied in a continuous manner to cover all spatial frequencies. As an example, we set the length of the heterostructure and the resulting 2DEG channel to be $2 \mu\text{m}$ in the simulation. Like any resonating structure, the plasmonic modes of the 2DEG channel are well-defined.^{31–33} Figure 3 shows simulations of plasmonic standing waves generated by a current-driven instability in the plasma channel (COMSOL). Here, the effective dielectric function of the 2DEG can be expressed as $\epsilon(\omega_p) = \epsilon_s - j\sigma_s/(\omega_p \Delta)$,³⁴ where Δ is the

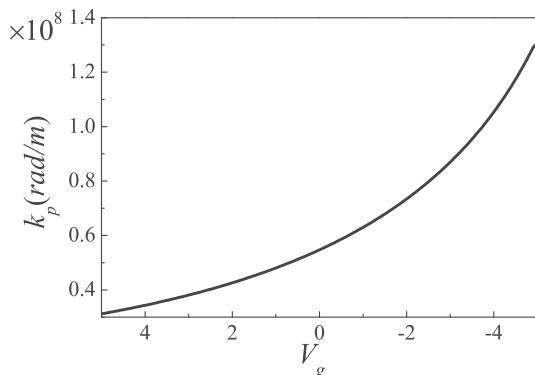


FIG. 2. Plasmon wave dispersion diagram for a transistor structure supporting a 2DEG channel. Here, $V_T = -9$ V, $h = 20$ nm, and $d = 120$ nm.

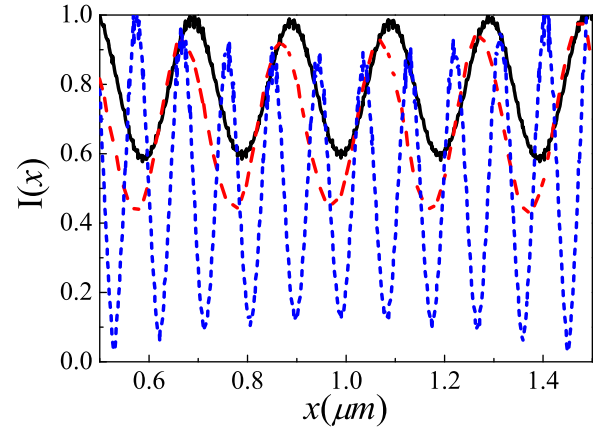


FIG. 3. Full-wave simulation results: Standing plasmonic wave patterns generated by a current-driven instability and an additional illumination at an angle χ . The field intensities are normalized. The surface current intensity is 1 mA/m, and the incident wave amplitude is 0.5 V/m. The black solid and blue short dashed curves have incident angles $\chi = 0$, while the red dashed curve has an incident angle of $\chi = 0.245$ rad. The corresponding gate voltages of the black solid, red dashed, and blue short dashed curves are 5, 5, and -0.4 V, respectively.

2DEG thickness and is set to be 2 nm in our simulations. Due to the huge value of the plasmonic wave number, the electric fields along the x direction and the z direction of a plasmon near the 2DEG have almost the same amplitude but a phase difference $\pi/2$. Two counter-propagating plasmons along the 2DEG have a z component proportional to $e^{jk_p x} \mathbf{e}_z + e^{-jk_p x} \mathbf{e}_z = 2 \cos(k_p x) \mathbf{e}_z$ and an x component proportional to $e^{jk_p x} \mathbf{e}_x - e^{-jk_p x} \mathbf{e}_x = 2 \sin(k_p x) \mathbf{e}_x$. The total field intensity has a constant intensity along the x direction.³⁵ If a plane wave $E_a (\cos \chi \mathbf{e}_x + \sin \chi \mathbf{e}_z) e^{jk_0 \sin \chi x}$ with incident angle χ and amplitude $E_a = E_0 e^{j\theta}$ illuminates the sample at the same time, the total field intensity on the sample can be approximated as

$$\begin{aligned} & |2 \cos(k_p x) + E_a \cos \chi e^{jk_0 \sin \chi x}|^2 \\ & + |2 \sin(k_p x) + E_a \sin \chi e^{jk_0 \sin \chi x}|^2 \\ & = 4 + |E_a|^2 + 4E_0 \cos(\sin \chi k_0 x + \theta) \cos(k_p x - \chi). \end{aligned} \quad (1)$$

Due to $\sin \chi k_0 \ll k_p$, we can neglect the coefficient $\cos(\sin \chi k_0 x)$. The above expression describes a standing wave pattern with an effective period of $2\pi/k_p$. More remarkably, the phase shift can be controlled by the incident angle. The simulations in Fig. 3 also show that the standing wave patterns can be obtained and shifted by the surface current and an additional plane wave incident from above.

In a linear SIM based on the surface plasmon structure described above, the illumination pattern $I(\mathbf{r})$ can be assumed to be sinusoidal and expressed as $I(\mathbf{r}) = C + (e^{jk_p \cdot \mathbf{r} + j\phi} + e^{-jk_p \cdot \mathbf{r} - j\phi})$, where C is a constant background, \mathbf{k}_p is the plasmonic wavevector, and ϕ is the pattern phase. An image $M(\mathbf{r})$ of a sample molecule distribution $F(\mathbf{r})$ observed using a microscope can be expressed as

$$M(\mathbf{r}) \propto \int F(\mathbf{r}') I(\mathbf{r}') H(\mathbf{r} - \mathbf{r}') d\mathbf{r}', \quad (2)$$

where $H(\mathbf{r})$ is the point spread function (PSF) of the microscope. A spatial frequency domain representation of the image

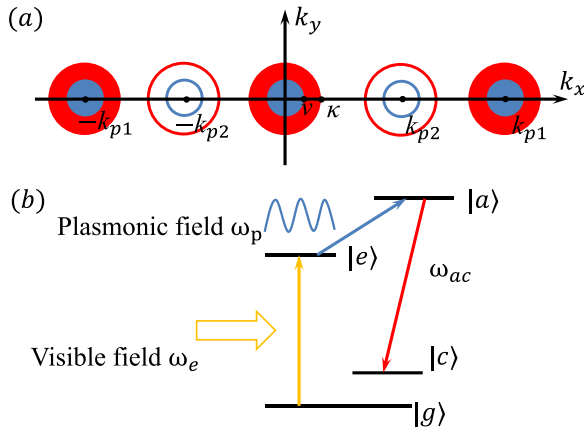


FIG. 4. (a) Diagram of the spatial frequency distributions. The blue and red circles at the origin contribute to the conventional microscopy with imaging frequencies ω_p and ω_{ac} , respectively. The circles with the center at $\pm k_{p1}/2$ correspond to the linear response of the illumination pattern with period $2\pi/k_{p1/2}$. The period of the illuminating plasmons can be tuned by the gate voltage. (b) The energy structure of the sample molecule.

obtained by taking the Fourier transform is expressed as $\tilde{M}(\mathbf{k}) = \tilde{F}(\mathbf{k})\tilde{H}(\mathbf{k})$, where \sim indicates a spatial frequency domain term, $\tilde{H}(\mathbf{k})$ is the optical transfer function (OTF) of the microscopy, and $\tilde{F}(\mathbf{k})$ is the Fourier transform of $F(r)I(r)$. A spatial frequency representation of the scheme is illustrated in Fig. 4(a). In this scheme, we assume that the numerical aperture of the objective lens is unity. In conventional fluorescence microscopy, the observable spatial frequency is limited to the circular region shown in Fig. 4(a) where the passband is bound by $(k_x^2 + k_y^2)^{1/2} = 2k_0 = 2\omega_p/c = \nu$. Since the plasmon frequency ω_p falls in the terahertz region, a relatively small k_0 implies that we need to image the sample a large number of times, which is time consuming. The process can be expedited by using an additional illumination field such as a laser with frequency ω_e . As shown in Fig. 4(b), the molecules in the sample are first excited from the ground level $|g\rangle$ to the excited level $|e\rangle$ by laser ω_e . The plasmonic wave then excites the molecules to an ancilla level $|a\rangle$. Utilizing the spontaneous decay of the molecules from $|a\rangle$ to $|c\rangle$, we image the sample with photons of frequency $\omega_{ac} = \omega_a - \omega_e$. A frequency-selective photonic crystal placed behind the objective lens can filter photons of different frequencies.⁴ As a consequence, the resulting passband in the spatial frequency domain is now bound by $(k_x^2 + k_y^2)^{1/2} = 2k_{ac} = 2\omega_{ac}/c = \kappa$, which is the larger circle illustrated in Fig. 4(a). Since κ is much larger than ν , high resolution can be realized by imaging the sample only a few times.

A sinusoidal illumination pattern has three frequency components which, along with two shifted versions as shown in Fig. 4(a), generate an image from a linear combination of this frequency information. To reconstruct the sample, three different images need to be captured with each possessing a different phase term ϕ . The process can be expressed as a system of linear equations

$$\tilde{F}(\mathbf{k}) = C\tilde{f}(\mathbf{k}) + \tilde{f}(\mathbf{k} - \mathbf{k}_p)e^{j\phi} + \tilde{f}(\mathbf{k} + \mathbf{k}_p)e^{-j\phi}. \quad (3)$$

The phase shifts ϕ are known beforehand. The frequency content of the sample up to $k_p + \kappa$ can therefore be observed due to the *Moiré* effect which transports the high frequency information into the observation region. In order to obtain

the three components of the spatial frequency as shown in the above equation, we need to shift the plasmonic patterns. Our simulation results show that an additional incident plane wave can shift the pattern effectively. In Fig. 3, the red dashed curve shows the shift of the standing wave. Slight changes of the incident angles result in different phase variations which are needed to solve the spatial frequency in Eq. (3). To achieve two-dimensional enhancement in resolution, we can illuminate the sample with different angles and a real setup will be given in the following.

Efficient production of plasmons with discrete wave numbers is accomplished due to the resonator effect in the transistor channel. The mode separation can be approximated as $\Delta_k = 2\pi \times 10^6$ rad/m. Thus, full coverage of all the spatial frequencies cannot be accomplished just by tuning the plasmonic wavelengths. However, as discussed earlier, through the larger circle shown in Fig. 4(a), all the spatial frequencies up to the plasmonic wavenumber can be recovered. For a laser frequency ω_e with a wavelength of 600 nm, the circle radius is $\kappa = 4\pi/6 \times 10^7$ rad/m. Since $\Delta_k < \kappa$, all the spatial frequencies can be obtained.

The boundaries and loss in the 2DEG can cause irregularities in the field patterns. These irregularities mean that we cannot simply separate the spatial frequency into the three spatial frequency components in Eq. (3). However, if the sample size or even the transistor channel length is much smaller than the plasmon wave propagation length, i.e., $1/Im(k_p)$, the irregularities resulting from loss can be neglected. With ever improving nanofabrication processing techniques, the loss along the 2DEG channel can be very small, which subsequently means a large $Re(k_p)/Im(k_p)$ ratio. Additionally, in order to improve the accuracy of the spatial frequency components, we perform Fourier expansion on the field intensity, the components of which are shown in Fig. 5. The figure shows that only a few larger Fourier components have values big enough to overcome the noise. As a consequence, Eq. (3) has several more terms and we still can obtain the spatial frequencies just by imaging the sample several more times. In order to enlarge the image size, the structure can be designed as a honeycomb lattice with hexagonal sides as the drains and sources. The distance between two parallel sides can be set to $2 \mu\text{m}$, and the side length can

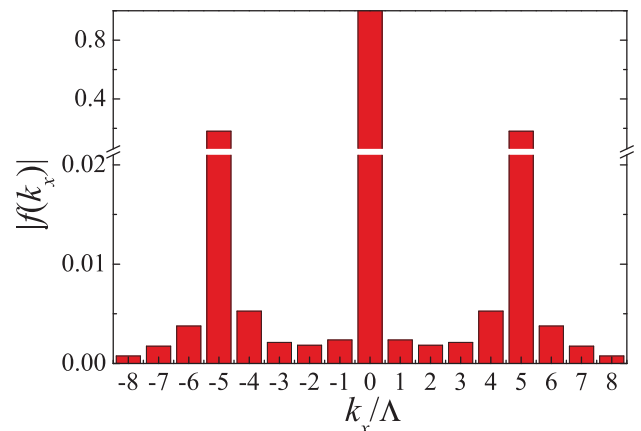


FIG. 5. The Fourier components of the red dashed line in Fig. 3. $\Lambda = 2\pi/S$, and $S = 1 \mu\text{m}$ is the size of the sample along x .

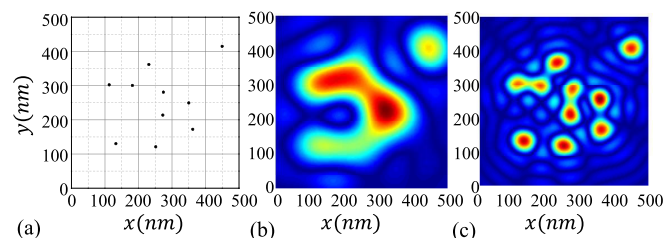


FIG. 6. (a) Sample distribution. Simulation of the reconstructed sample image with parameters: (b) $Re(k_p^{max}) = 100k_0$ and (c) $Re(k_p^{max}) = 300k_0$.

be set to $1 \mu\text{m}$. The voltage difference between two parallel sides can generate surface plasmons. The 3 pairs of parallel sides can realize 3 illumination angles. Due to the periodicity of the structure, we can do two dimensional Fourier expansions on the field distribution, where we can nearly obtain all the spatial frequency information in our following simulation cases. Of course, the complexity of the structure brings challenge to the fabrication and subsequently the irregularity of the illumination field. A mathematical algorithm used in Refs. 9 and 36, called blind-SIM, can be used to solve the spatial frequencies.

With all the Fourier information known now, an image of the sample can be reconstructed. We consider a sample with molecule distribution shown in Fig. 6(a). The minimum separation between the molecules is about 70 nm. The 2DEG plasmons have a frequency of 10THz, and the numerical aperture (NA) is assumed to be 1. The reconstruction involves contributions from the spatial content up to a circular region of radius $k_p + \kappa$, where k_p can be manipulated by gate voltage. In Figs. 6(b) and 6(c), images with maximum plasmonic wavenumber 100 and 300 times larger than the vacuum wavenumber are shown corresponding to 150 and 75 nm resolution, respectively. Figure 6(b) shows that particles separated by a distance less than 150 nm cannot be resolved and appear as a contiguous blurry streak, whereas they are distinguishable in Fig. 6(c). This demonstrates that our schema can technically obtain extremely high resolution.

Due to the large circle radius κ shown in Fig. 4(a), a total of only 20–40 images are required for the final image reconstruction, which in terms of imaging speed is very fast and is comparable to traditional nonlinear SIM.⁴ However, unlike nonlinear SIM, the method described here requires only weak illumination intensity.

In this paper, we have proposed a super-resolution microscopy scheme based on the subwavelength surface electromagnetic plasmons found in a semiconductor heterostructure. This method is useful in particular for light-sensitive samples that require weak field intensity for illumination. Compared to metal based SIM where the plasmonic wavelengths are fixed, the plasmonic pattern can be controlled by varying the gate voltage. Moreover, compared to the scheme based on graphene,¹¹ our method uses surface current to excite the plasmons, no complex wavevector

matching structure is needed, and it can be more easily realized in experiment.

This research was supported by National Priorities Research Program (NPRP) Grant No. 8-352-1-074 from the Qatar National Research Fund (QNRF).

- ¹M. G. L. Gustafsson, *J. Microsc.* **198**, 82–87 (2000).
- ²R. Heintzmann and C. G. Cremer, *Proc. SPIE* **3568**, 185–195 (1999).
- ³R. Heintzmann and G. Ficz, *Briefings Funct. Genomics Proteomics* **5**, 289–301 (2006).
- ⁴M. G. L. Gustafsson, *PNAS* **102**, 13081–13086 (2005).
- ⁵X. Zeng, M. Al-Amri, Z. Liao, and M. S. Zubairy, *Phys. Rev. A* **91**, 063811 (2015).
- ⁶F. Wei and Z. Liu, *Nano Lett.* **10**, 2531–2536 (2010).
- ⁷F. Wei, D. Lu, H. Shen, W. Wang, J. L. Ponsetto, E. Huang, and Z. Liu, *Nano Lett.* **14**, 4634–4639 (2014).
- ⁸J. L. Ponsetto, F. Wei, and Z. Liu, *Nanoscale* **6**, 5807 (2014).
- ⁹J. L. Ponsetto, A. Bezryadina, F. Wei, K. Onishi, H. Shen, E. Huang, L. Ferrari, Q. Ma, Y. Zou, and Z. Liu, *ACS Nano* **11**, 5344 (2017).
- ¹⁰A. I. Fernández-Domínguez, Z. Liu, and J. B. Pendry, *ACS Photonics* **2**, 341 (2015).
- ¹¹X. Zeng, M. Al-Amri, and M. S. Zubairy, *Phys. Rev. B* **90**, 235418 (2014).
- ¹²A. B. Mikhailovskii, *Theory of Plasma Instabilities* (Springer, 2013).
- ¹³K. Kempa, P. Bakshi, J. Cen, and H. Xie, *Phys. Rev. B* **43**, 9273 (1991).
- ¹⁴G. C. Dyer, X. Shi, B. V. Olson, S. D. Hawkins, J. F. Klem, E. A. Shaner, and W. Pan, *Appl. Phys. Lett.* **108**, 013106 (2016).
- ¹⁵J. Wu, A. S. Mayorov, C. D. Wood, D. Mistry, L. Li, W. Muchenje, M. C. Rosamond, L. Chen, E. H. Linfield, A. G. Davies et al., *Sci. Rep.* **5**, 15420 (2015).
- ¹⁶F. Stern, *Phys. Rev. Lett.* **18**, 546 (1967).
- ¹⁷S. J. Allen, Jr., D. C. Tsui, and R. A. Logan, *Phys. Rev. Lett.* **38**, 980 (1977).
- ¹⁸M. Dyakonov and M. Shur, *Phys. Rev. Lett.* **71**, 2465 (1993).
- ¹⁹M. Dyakonov and M. Shur, *IEEE Trans. Electron Devices* **43**, 380–387 (1996).
- ²⁰V. V. Popov, G. M. Tsymbalov, M. S. Shur, and W. Knap, *Semiconductors* **39**, 142–146 (2005).
- ²¹T. Otsuji, M. Hanabe, T. Nishimura, and E. Sano, *Opt. Express* **14**, 4815–4825 (2006).
- ²²M. Dyakonov and M. S. Shur, *Appl. Phys. Lett.* **87**, 111501 (2005).
- ²³D. Hofstetter, L. Diehl, J. Faist, W. J. Schaff, J. Hwang, L. F. Eastman, and C. Zellweger, *Appl. Phys. Lett.* **80**, 2991 (2002).
- ²⁴A. E. Fatimy, N. Dyakonova, Y. Meziani, T. Otsuji, W. Knap, S. Vandenbrouk, K. Madjour, D. Théron, C. Gaquiere, M. A. Poisson et al., *J. Appl. Phys.* **107**, 024504 (2010).
- ²⁵S. Rabbaa and J. Stiens, *J. Phys. D: Appl. Phys.* **44**, 325103 (2011).
- ²⁶R. Kastner, E. Heyman, and A. Sabban, *IEEE Trans. Antennas Propag.* **36**, 1204–1212 (1988).
- ²⁷K. A. Michalski, *Encyclopedia of RF and Microwave Engineering* (John Wiley & Sons, Inc., 2005).
- ²⁸P. J. Burke, I. B. Spielman, J. P. Eisenstein, L. N. Pfeiffer, and K. W. West, *Appl. Phys. Lett.* **76**, 745 (2000).
- ²⁹M. Nakayama, *J. Phys. Soc. Jpn.* **36**, 393–398 (1974).
- ³⁰A. Eguiluz, T. K. Lee, J. J. Quinn, and K. W. Chiu, *Phys. Rev. B* **11**, 4989 (1975).
- ³¹A. V. Muravjov, D. B. Veksler, V. V. Popov, O. V. Polischuk, N. Pala, X. Hu, R. Gaska, H. Saxena, R. E. Peale, and M. S. Shur, *Appl. Phys. Lett.* **96**, 042105 (2010).
- ³²V. V. Popov, A. N. Koudymov, M. Shur, and O. V. Polischuk, *J. Appl. Phys.* **104**, 024508 (2008).
- ³³V. V. Popov, M. S. Shur, G. M. Tsymbalov, and D. V. Fateev, *Int. J. High Speed Electron. Syst.* **17**, 557–566 (2007).
- ³⁴T. Ando, A. B. Fowler, and F. Stern, *Rev. Mod. Phys.* **54**, 437 (1982).
- ³⁵X. Zeng, L. Fan, and M. S. Zubairy, *Phys. Rev. A* **95**, 053850 (2017).
- ³⁶E. Mudry, K. Belkebir, J. Girard, J. Savatier, E. Le Moal, C. Nicoletti, M. Allain, and A. Sentenac, *Nat. Photonics* **6**, 312–315 (2012).